

# Plasma and Terahertz-Wave Propagation Characteristics in Atmospheric-Pressure Plasma Jet Under Different Operating Conditions

Wenchong Ouyang<sup>✉</sup>, *Graduate Student Member, IEEE*, Qi Liu, Wenzhe Mao<sup>✉</sup>, Shuzhan Gao, and Zhengwei Wu<sup>✉</sup>, *Member, IEEE*

**Abstract**— High-density plasma source device is of great significance for ground experiment verification of vehicle reentry communication. Atmospheric-pressure plasma jet (APPJ), as a high-density plasma source, has received little attention in ground experiments on vehicle communications. In this article, terahertz (THz)-wave propagation characteristics in APPJ are investigated by joint simulation of APPJ discharge and THz transport model and related experimental measurements. THz interferometer (THz-IF) system is used to diagnose the electron density and THz transmission characteristics of APPJ for the first time, and the measured results are in good agreement with the simulation results of a joint simulation model in this article and the measured results of THz time-domain spectroscopy (THz-TDS) system of other researchers. Sheath thickness and electron density produced by self-designed APPJ are highly matched with the plasma sheath environment of the HIFIRE-5b vehicle. Further analysis of the influence of different voltages and needle electrode radius on the THz transmission characteristics shows that the absorption effect plays a major role in THz-wave attenuation in APPJ, and the contribution of the collision effect almost disappears, which is completely consistent with the phenomenon observed in HIFIRE-5b vehicle. The joint simulation model and THz-IF method developed in this article are of great significance for the ground test verification of reentry communication schemes.

**Index Terms**— Electromagnetic wave polarization hypersonic vehicles, plasma diagnostics, plasma jets, terahertz (THz) communications, THz wave absorption.

## I. INTRODUCTION

DURING returning the capsule of spacecraft reentering, a plasma sheath covering the capsule surface is formed

Manuscript received 9 August 2022; revised 5 December 2022; accepted 13 December 2022. Date of publication 23 January 2023; date of current version 6 March 2023. This work was supported in part by the International Thermonuclear Experimental Reactor (ITER) Project of the Ministry of Science and Technology under Grant 2022YFE03080001, in part by the Fundamental Research Funds for the Central Universities under Grant WK5290000002, and in part by the Joint Laboratory of Plasma Application Technology Funding under Grant JL06120001H. (*Corresponding author: Zhengwei Wu*)

The authors are with the School of Nuclear Science and Technology, University of Science and Technology of China, Hefei 230026, China (e-mail: oywc13978384979@gmail.com; qliu15@mail.ustc.edu.cn; maozhe@ustc.edu.cn; gsz@mail.ustc.edu.cn; wuzw@ustc.edu.cn).

Color versions of one or more figures in this article are available at <https://doi.org/10.1109/TAP.2023.3237284>.

Digital Object Identifier 10.1109/TAP.2023.3237284

due to intense friction with the thin air [1]. The plasma sheath will adversely affect the communication signals between the vehicle and ground base station, such as attenuation, phase shift, and delay in communications and radar signals. And radio frequency (RF) blackout will occur in severe cases [2]. To alleviate and even solve the RF blackout problem, scientists have conducted extensive research and proposed a series of methods [3], [4], [5], [6]. Among them, terahertz (THz) communication is considered a potential solution with engineering feasibility due to its high-frequency performance and the rapid development of THz sources [7], [8].

The core basis of the THz communication scheme for RF blackout is the interaction between THz wave and plasma, which has received extensive attention in recent years. Tian et al. [9] investigated the effect of collision frequency inhomogeneity on the THz transmission properties in non-magnetized plasmas. Chen et al. [10] studied the THz transmission characteristics in real reentry plasma sheaths under different wave frequencies and antenna positions by using the hypersonic fluid model and scattering matrix method (SMM). Gradually, the effects of specific external parameters such as atmospheric conditions, flight parameters, and vehicle shape on the plasma sheath and THz communication have been studied. Yuan et al. [11] studied the effect of atmospheric conditions on the THz-wave attenuation and obtained geographic differences in global THz signal propagation. Yang et al. [12] and Zhang et al. [13] studied the effect of flight speed and the angle of attack on the transmission coefficient of THz waves and analyzed the corresponding change law. Ouyang et al. [14] and Tang et al. [15] numerically analyzed differences in THz transmission characteristics under different vehicles and determined the corresponding THz communication frequency.

With the development of plasma source devices, the propagation characteristics of THz waves in high-density plasma generated by plasma sources have gradually attracted attention. Jang et al. [16] employed THz time-domain spectroscopy (THz-TDS) to diagnose electron density and collision frequency information in an inductively coupled plasma (ICP) source and analyzed the effects of RF power and gas pressure on electron density [17]. Sun et al. [18] verified the feasibility of ICP and THz-wave transmission combined model

based on THz-TDS and laser Thomson scattering method, and the effect of RF power and gas pressure on the THz transmission characteristics in ICP was further discussed. The plasma sources concerned in the above THz-wave transmission research studies are all ICP devices due to their high-density characteristics. Atmospheric-pressure plasma jet (APPJ) devices, whose plasma environment (electron density is as high as  $10^{19} \text{ m}^{-3}$  or even  $10^{20} \text{ m}^{-3}$ ) [19], [20] is very close to the reentry plasma sheath [14], [15], which has almost not been paid attention to in THz transmission research. Chen et al. [21] used THz-TDS technology to diagnose the electron density of helium plasma jets and measured the transmittance of THz waves in the plasma jet. However, the electron density of APPJ needs to be further diagnosed by theoretical models and more measurement methods to verify the matching with the reentry plasma sheath environment. Moreover, the transmission characteristics of THz wave in APPJ under different conditions (such as discharge voltage and electrode radius) also need to be further studied to explore whether the THz attenuation contribution mechanism in APPJ device is consistent with the reentry plasma environment. This article primarily verifies the feasibility of APPJ equipment applied to the ground experiment of reentry communication by solving the above two problems.

THz interferometer (THz-IF) system, as a mature technology applied to the diagnosis of fusion plasma, has the advantages of high precision, high-temperature, and high-density diagnosis [22]. Although the high electron density of fusion plasma is similar to the environment of APPJ and reentry plasma sheath, the THz-IF system has not been used to diagnose the environment of APPJ and the measurement of THz transmission characteristics in APPJ so far. Moreover, different plasma diagnostic environments will lead to significant differences in the theoretical basis and experimental requirements of diagnosis. For example, the THz attenuation data are insensitive and the test optical path is difficult to calibrate due to the low plasma sheath thickness of APPJ. Therefore, this work provides a new diagnostic method for the plasma environment of APPJ. More importantly, it is of great significance to the ground test verification of the reentry communication scheme for APPJ and plasma-jet-type wind tunnels in the future.

In this article, plasma generated by helium APPJ is used to match a high-density plasma sheath of the same magnitude, and an innovative method combining the APPJ discharge model and the THz transport model is proposed. First, the electron density under different voltages simulated by the APPJ model is compared with the diagnostic results of the THz-IF system in this article, as well as the THz-TDS diagnostic results of other researchers, and the comparison results are in good agreement. Then, the effect of different voltages and needle electrode radius on the electron density is analyzed. Finally, the simulation results obtained from the joint simulation of APPJ discharge and THz-wave transmission model are in good agreement with the experimental results by the THz-IF system, and the effect of voltages and needle electrode radius on the propagation characteristics of THz wave is further discussed.

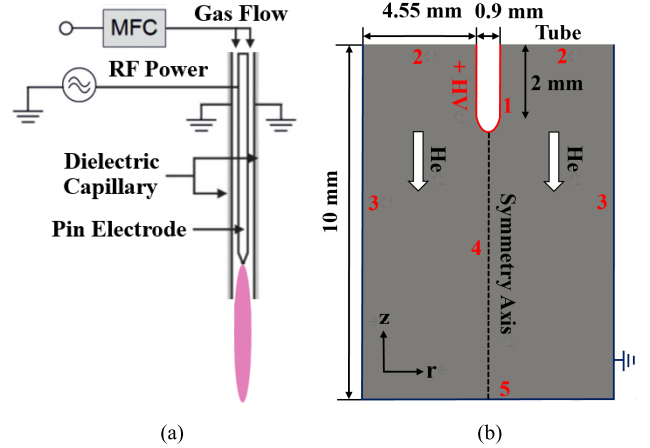


Fig. 1. (a) Structural diagram. and (b) simulation domain of APPJ.

## II. DESCRIPTION OF THEORY MODEL

### A. APPJ Discharge Model

Fig. 1 shows the structural diagram and simulation domain of APPJ in this work. A needle electrode is embedded in the medium tube, and both ends of the medium tube are grounded. The radius of the needle electrode and medium tube are 0.45 and 5.0 mm, respectively. A pulsed dc voltage with a rising edge of 140 ns is applied to the needle electrode. And the discharge voltage is 4.0–5.8 kV. When helium gas is passed into the dielectric tube, high-density plasma is formed under the high-voltage (HV) discharge between the needle electrode and the dielectric tube.

A 2-D fluid model [19] coupled with the reaction rates and electron transport coefficients obtained by the BOLSIG<sup>+</sup> solver [23] was applied to solve the discharge characteristics of APPJ based on COMSOL Platform. The electron density and electron energy are described by the continuity equation and energy conservation equation, respectively,

$$\frac{\partial n_e}{\partial t} + \nabla \cdot \vec{\Gamma}_e = s_e \quad (1)$$

$$\frac{\partial n_\varepsilon}{\partial t} + \nabla \cdot (-n_\varepsilon(\mu_\varepsilon \vec{E}) - D_\varepsilon \nabla n_\varepsilon) + \vec{E} \cdot \vec{\Gamma}_e = s_\varepsilon \quad (2)$$

$$\vec{\Gamma}_e = -n_e(\mu_e \vec{E}) - D_e \nabla n_e \quad (3)$$

where  $n_e$  and  $n_\varepsilon$  are the electron density and electron energy density,  $s_e$  and  $s_\varepsilon$  represent the source term of electron and electron energy, and  $\vec{E}$  is the electric field.  $D_e$  and  $D_\varepsilon$  refer to the diffusion coefficients of electron and electron energy, which can be expressed as

$$D_e = \mu_e T_e, \quad D_\varepsilon = \mu_\varepsilon T_e. \quad (4)$$

Electron energy mobility coefficient  $\mu_e$  and electron mobility coefficient  $\mu_\varepsilon$  satisfy the following relationship, and electron mobility coefficient is solved by BOLSIG<sup>+</sup> [23]:

$$\mu_e = \frac{5}{3} \mu_\varepsilon. \quad (5)$$

TABLE I  
BOUNDARY CONDITIONS OF SIMULATION MODEL

	1	2	3	4	5
$n_e$	Eq. (10)	$\frac{\partial n_e}{\partial z} = 0$	Eq. (10)	$\frac{\partial n_e}{\partial r} = 0$	Eq. (10)
$n_i$	Eq. (11)	$\frac{\partial n_i}{\partial z} = 0$	Eq. (11)	$\frac{\partial n_i}{\partial r} = 0$	Eq. (11)
$n_m$	Eq. (12)	$\frac{\partial n_m}{\partial z} = 0$	Eq. (12)	$\frac{\partial n_m}{\partial r} = 0$	Eq. (12)
$n_e$	Eq. (13)	$\frac{\partial n_e}{\partial z} = 0$	Eq. (13)	$\frac{\partial n_e}{\partial r} = 0$	Eq. (13)
$\Phi$	$V$	$\frac{\partial \Phi}{\partial z} = 0$	Eq. (15)	$\frac{\partial \Phi}{\partial r} = 0$	0

Electron energy source term  $s_e$  can be calculated by the collision energy loss from related chemical reactions

$$s_e = -s \sum_j \Delta E_j K_{inel,j} - 2n_i k_B \frac{m_e}{M_i} (T_e - T_g) v_e \quad (6)$$

where  $\Delta E_j$  is the energy loss from reaction  $j$ .  $K_{inel,j}$  refers to the reaction rate of reaction  $j$ , which can be obtained from BOLSIG<sup>+</sup> [23].  $k_B$  and  $m_e$  are Boltzmann's constant and electron mass, and the corresponding values are  $1.38 \times 10^{-23}$  J/K and  $9.109 \times 10^{-31}$  kg, respectively.  $M_i$  is the heavy species mass and  $T_e$  and  $T_g$  represent the temperature of electrons and gas.  $v_e$  refers to the collision frequency between electrons and neutral particles, which can be estimated by [24]

$$v_e = 2.6 \times 10^4 n_n r^2 T_e \quad (7)$$

where  $n_n$  and  $r$  represent the neutral particle density and electron-neutral collisional radius.

The electron temperature and electric field can be solved by

$$T_e = \frac{2}{3k_B} \frac{n_e}{n_e} \quad (8)$$

$$\nabla \cdot (\epsilon \vec{E}) = \sum_{i=1}^N q_i n_i - e n_e \quad (9)$$

where  $\epsilon$  is the permittivity.

The boundary conditions in the simulation domain are shown in Table I, and the values 1–5 marked in red in Fig. 1 correspond to different boundary conditions. The boundary conditions for particle flux  $\Gamma$  and electron energy density at the different boundaries can be expressed as

$$\vec{E}_e \cdot \vec{n} = \frac{1}{4} n_e \sqrt{\frac{8k_B T_e}{\pi m_e}} - \alpha_s \sum_i \gamma_i (\vec{\Gamma}_i \cdot \vec{n}) + \alpha'_s \mu_e n_e \vec{E} \quad (10)$$

$$\vec{\Gamma}_i \cdot \vec{n} = \frac{1}{4} n_i \sqrt{\frac{8k_B T_i}{\pi m_i}} + \alpha'_s \mu_e n_e \vec{E} \quad (11)$$

$$\vec{\Gamma}_m \cdot \vec{n} = \frac{1}{4} n_m \sqrt{\frac{8k_B T_g}{\pi m_m}} \quad (12)$$

$$\vec{\Gamma}_e \cdot \vec{n} = \frac{1}{2} n_e \sqrt{\frac{8k_B T_e}{\pi m_e}} - 2\alpha_s k_B T_e \sum_i \gamma_i (\vec{\Gamma}_i \cdot \vec{n}) \quad (13)$$

where  $\vec{n}$  refers to the normal vector pointing to the surface and  $n$  and  $m$  represent the density and mass of a particle.

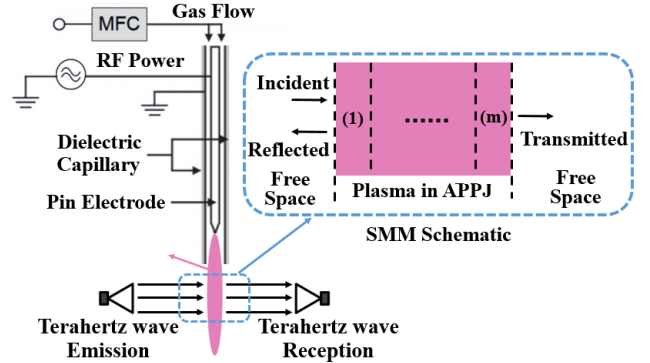


Fig. 2. Schematic of SMM used for THz transmission in APPJ.

$\gamma$  refers to the secondary electron emission coefficient.  $\alpha_s$  and  $\alpha'_s$  can be obtained from the following equation:

$$\alpha_s = \begin{cases} 0 & (\vec{E} \cdot \vec{n} < 0) \\ 1 & (\vec{E} \cdot \vec{n} \geq 0) \end{cases} \quad \alpha'_s = \begin{cases} 1 & (\vec{E} \cdot \vec{n} < 0) \\ 0 & (\vec{E} \cdot \vec{n} \geq 0). \end{cases} \quad (14)$$

The self-bias potential on the surface of the dielectric tube can be calculated by Gauss's law

$$(\vec{D}_2 - \vec{D}_1) \cdot \vec{n} = \sigma_s \frac{d\sigma_s}{dt} = (\vec{\Gamma}_e + \vec{\Gamma}_i) \cdot \vec{n} \quad (15)$$

where  $\sigma_s$  and  $\vec{D}$  represent net surface charge accumulated and electric displacement on the dielectric surface, respectively.

In a real helium plasma jet experiment, impurities from a gas tank or pipeline mix with helium, causing a mixture of helium, air, nitrogen, and oxygen to escape. At the same time, helium plasma will interact with the ambient air again at the outlet of the capillary. The previous studies have confirmed that the Penning ionization of helium molecules to nitrogen molecules plays a key role in the properties of the plasma jet [25], [26], and there are also significant differences in the effects of different contents of nitrogen and oxygen on the plasma jet [27], [28]. At present, the content of air, N<sub>2</sub>, O<sub>2</sub>, and the specific reactions in the helium plasma jet are very complex and there is no clear standard. Therefore, pure helium was considered in this article, the corresponding chemical reactions are consistent with the previous studies [19]. In the present simulation, the initial pressure and temperature are set to 1 atm and 300 K, respectively, and high-precision mesh (the number of meshes is 239 220) is divided to describe the complex chemical reaction and discharge process. The distribution of parameters such as electron density, electron energy, and electron temperature of APPJ discharge can be obtained by solving the above model.

### B. THz-Wave Transmission Model in APPJ

For nonmagnetized plasmas in APPJ, the SMM [15] is employed to solve the THz transmission properties in APPJ. The core idea of SMM is to divide the plasma in APPJ into multiple uniform thin layers, as shown in Fig. 2.

The plasma of each layer is regarded as a lossy medium, and the relative permittivity  $\epsilon_r$  of each layer can be solved

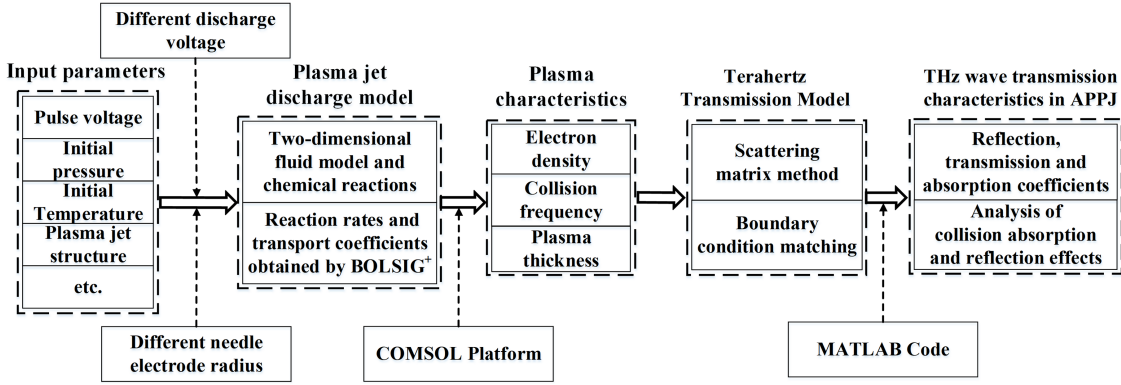


Fig. 3. Algorithm flowchart of the joint simulation model of the APPJ discharge and THz transmission.

according to the corresponding electron density and collision frequency data

$$\varepsilon_{r,m} = 1 - \frac{(w_p/v_e)^2}{1 + (w/v_e)^2} - j \frac{w_p^2/wv_e}{1 + (w/v_e)^2} \quad (16)$$

where  $w$  is the angular frequency of THz wave and  $w_p$  refers to the plasma frequency, which is determined by the electron density

$$w_p = \sqrt{\frac{n_e q^2}{m_e \epsilon_0}}. \quad (17)$$

According to the relative permittivity of each layer, the corresponding wavenumber can be obtained

$$k_m = k_0 (\varepsilon_{r,m})^{\frac{1}{2}}, \quad k_0 = \frac{w}{c}. \quad (18)$$

The transmission characteristics of THz waves in APPJ are expressed in matrix form

$$S_g = \prod_{m=1}^m S_m = (S_{g1} \quad S_{g2}). \quad (19)$$

The scattering matrix of each layer can be described as

$$S_m = \begin{pmatrix} 1 & 1 \\ k_m & -k_m \end{pmatrix}^{-1} \begin{pmatrix} e^{-jk_{m-1}d} & e^{jk_{m-1}d} \\ k_{m-1}e^{-jk_{m-1}d} & -k_{m-1}e^{jk_{m-1}d} \end{pmatrix} \quad (20)$$

where  $d$  represents the thickness of each layer. By coupling the electromagnetic boundary conditions of adjacent thin layers, the THz reflection coefficient  $R$  and transmission coefficient  $T$  in the APPJ can be obtained

$$\begin{pmatrix} R \\ T \end{pmatrix} = - \begin{pmatrix} \frac{1}{2k_m}(k_m + k_{m+1})e^{j(k_m - k_{m+1})d} \\ \frac{1}{2k_m}(k_m - k_{m+1})e^{-j(k_m + k_{m+1})d} \end{pmatrix} S_{g1}. \quad (21)$$

Transmission, reflection, and absorption coefficients satisfy the relationship that sums to 1. Therefore, the absorption coefficient  $A$  of THz waves in APPJ is expressed as

$$A^2 = 1 - R^2 - T^2. \quad (22)$$

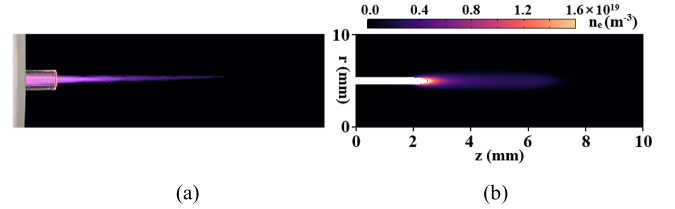


Fig. 4. Electron density distribution in helium APPJ. (a) Image of APPJ. (b) Simulation results.

### C. Joint Simulation Model of APPJ Discharge and THz Transmission

Based on the plasma jet discharge model and THz transmission model, a joint simulation model is developed to investigate the plasma characteristics and THz-wave propagation characteristics in APPJ under different operating conditions, the specific algorithm flow as shown in Fig. 3.

First, the plasma distribution of APPJ is solved by the plasma jet discharge, and the electron density, collision frequency, and plasma thickness data can be obtained from the plasma distribution. The corresponding transmission, reflection, and absorption coefficients are then solved by using these data as the input of the THz transmission model and matching the boundary electromagnetic conditions of the plasma layer with the SMM. Second, these data are used as the input of the THz transmission model, and the corresponding transmission, reflection, and absorption coefficients are solved by the SMM and boundary electromagnetic condition matching of the plasma layer. Finally, the effects of different voltages and needle electrode radius on the plasma characteristics and THz transmission characteristics are analyzed based on the above joint simulation model, and the contribution of absorption and reflection coefficients to the attenuation of THz transmission is discussed.

### III. MEASUREMENT AND SIMULATION OF PLASMA DENSITY IN APJJ DEVICE

#### A. Plasma Density Measurement in APPJ

Fig. 4 shows the photographs of APPJ discharge under pulsed dc voltage of 4.0 kV, the rising edge and pulsewidth are 140 ns and 2  $\mu\text{s}$ , respectively, and it changes periodically.

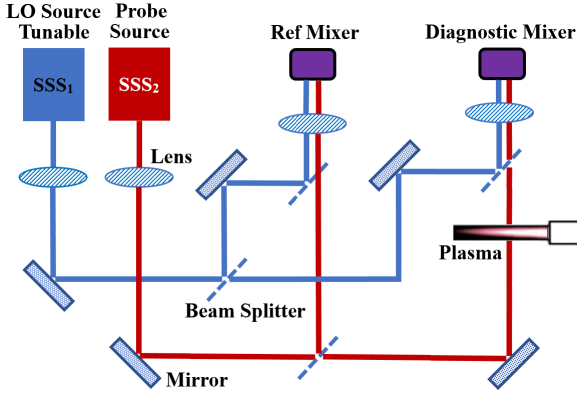


Fig. 5. Schematic of THz source interferometer systems used for measuring electron density in APPJ.

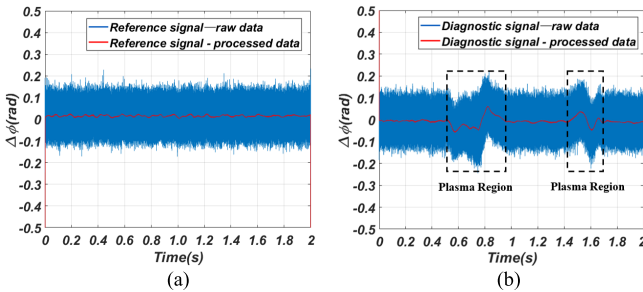


Fig. 6. Raw and processed phase data for (a) reference signal and (b) diagnostic signal in APPJ under discharge voltage of 5.0 kV.

The electron density distribution of the simulation results [see Fig. 4(b)] based APPJ discharge model has the same profile with the image of real APPJ discharge [see Fig. 4(a)]. And the electron density will be verified by numerical simulation (Fig. 4), phase variation measured by THz-IF systems (Fig. 6), and comparison with the THz-TDS diagnostic results (Fig. 7) in this section.

The THz-IF systems are shown in Fig. 5, and the stability and accuracy of the THz-IF system have been verified and reported in previous Keda Torus eXperiment (KTX) work (electron density on the order of  $10^{19} \text{ m}^{-3}$ ) [29], [30]. The solid-state sources  $\text{SSS}_1$  and  $\text{SSS}_2$  provide beams with different THz frequencies, and the frequencies of the two solid-state sources are 650 GHz and  $650 + \omega_{\text{IF}}$  GHz, respectively. The beam is reflected and transmitted through a lens or beam splitter to ensure the desired transmission path. Two pairs of beams passing and not passing through the plasma region in APPJ are received by the mixer, which corresponds to the reference signal detector (Ref Mixer) and the diagnostic signal detector (signal mixer), respectively.

The specific phase difference can be obtained by analyzing the phase changes of the reference signal  $\Delta\Phi_{\text{ref}}$  and the diagnostic signal  $\Delta\Phi_{\text{dia}}$ , the processed data are shown in Fig. 6. It is worth noting that the plasma jet travels back and forth through the signal diagnostic channel at a slow speed. Therefore, the phase difference data of the diagnostic signal only changes significantly during the round trip through the APPJ plasma region, as shown in Fig. 6(b).

The ratio of the reference signal wave to the diagnostic signal wave in the frequency domain is expressed

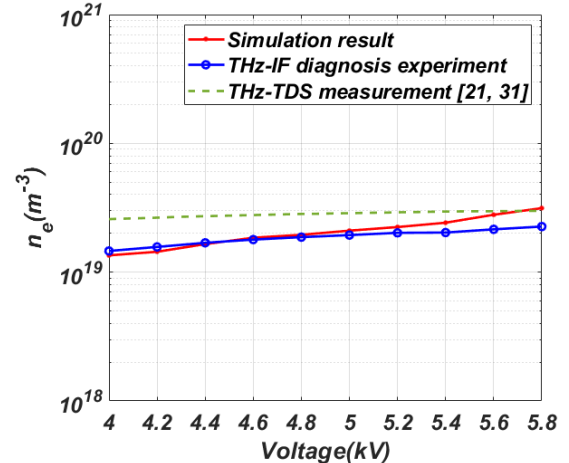


Fig. 7. Comparison of simulation results with the experimental results of THz-IF and THz-TDS diagnosis under different voltages.

as follows [21]:

$$\frac{E_{\text{dia}}(w)}{E_{\text{ref}}(w)} = \frac{4n_r(w)}{(n_r(w) + 1)^2} \exp\left(j \frac{(n_r(w) - 1)wd}{c}\right) \times \exp\left(-\frac{\chi(w)wd}{c}\right). \quad (23)$$

For the nonmagnetized cold plasma in APPJ, its relative permittivity can be transformed by (16) as

$$\varepsilon_r = \left(1 - \frac{w_p^2}{w^2 + v_e^2}\right) - j \frac{v_e}{w} \frac{w_p^2}{w^2 + v_e^2}. \quad (24)$$

The complex refractive index of the plasma can be obtained from the relative permittivity

$$n = \sqrt{\varepsilon_r} = n_r + j\chi \quad (25)$$

where  $n_r$  and  $\chi$  refer to the refractive index and extinction coefficient, respectively. The phase shift  $\Delta\Phi$  of the signal caused by the plasma is determined by the refractive index  $n_r$ .

The refractive index  $n_r$  can be obtained directly from the phase shift  $\Delta\Phi$  through (23) and (25)

$$\Delta\Phi = \frac{(n_r(w) - 1)wd}{c}. \quad (26)$$

Therefore, the electron density in APPJ can be obtained from the phase shift data of the reference and diagnostic signals

$$\Delta\Phi = \frac{wd}{c} \left(1 - \frac{w_p^2}{w^2 + v_e^2}\right)^{\frac{1}{2}}. \quad (27)$$

In (27),  $w$  refers to the angular frequency of THz waves,  $d$  represents the width of the plasma jet, which is about 4 mm, and  $w_p$  is related to electron density  $n_e$  and collision frequency  $v_e$ , as shown in (17). According to the phase data in Fig. 6, the electron density is obtained as  $1.94 \times 10^{19} \text{ m}^{-3}$ .

The simulation results of electron density in helium APPJ under different voltages are compared with the THz-IF and THz-TDS diagnostic results, as shown in Fig. 7. It needs to be clarified that the variation trend and ratio of electron density with voltage in the simulation results are in good

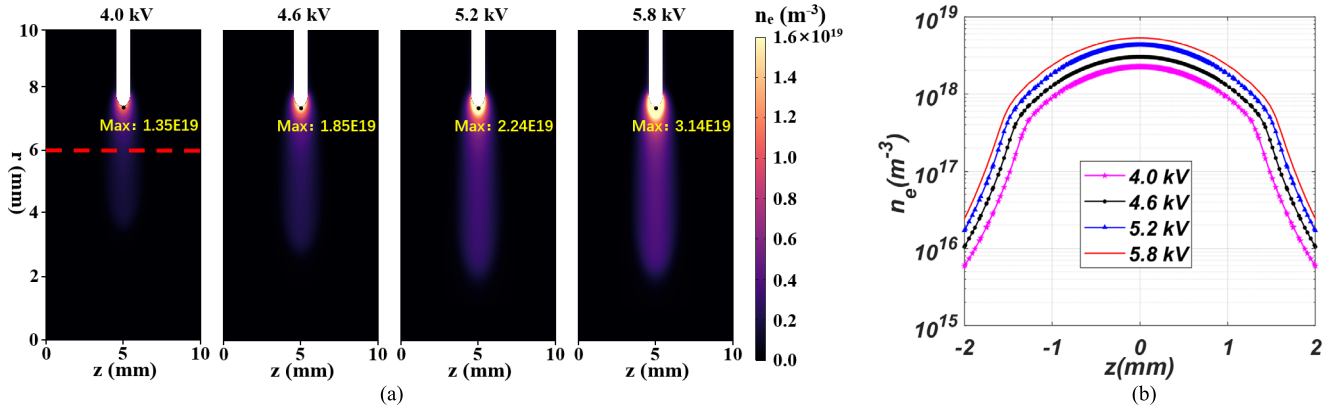


Fig. 8. (a) Global distribution of electron density in APPJ and (b) analysis of electron density along the THz-wave propagation path under different discharge voltages.

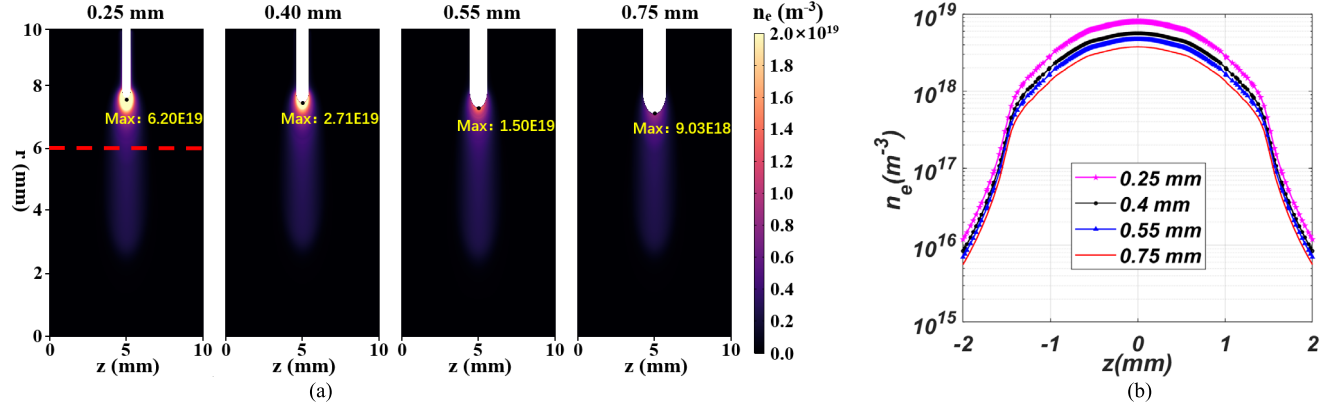


Fig. 9. (a) Global distribution of electron density in APPJ and (b) analysis of electron density along the THz-wave propagation path under needle electrode radius.

agreement with the THz-IF and THz-TDS experiments. Therefore, THz-IF and THz-TDS experimental results verify the reliability of the simulation results.

#### B. Simulation Analysis of Electron Density in APPJ Under Different Operating Conditions

The electron density distribution of APPJ was obtained by solving the 2-D fluid model, and the effects of discharge voltage and needle electrode radius on electron density are analyzed in this section. The rise time of applied forward pulse voltage is 1 ns, the discharge voltage ranged from 4.0 to 5.8 kV, and the needle electrode radius ranged from 0.25 to 0.75 mm.

Fig. 8(a) shows the electron density distribution in the APPJ under different voltages (needle electrode radius is 0.45 mm). It is obvious that the electron density increases with the discharge voltage, and the simulation results of electron density are in good agreement with the measurement results of the THz-TDS diagnostic system (Fig. 7) [21], [31]. When the discharge voltage increases from 4.0 to 5.8 kV, electron density increases from  $1.35 \times 10^{19} \text{ m}^{-3}$  to  $3.14 \times 10^{19} \text{ m}^{-3}$ . In addition, the APPJ length shows a trend of increasing first and then almost unchanged with the increase of voltage, which is consistent with the related experimental results [32], [33]. Fig. 8(b) further analyzes the electron density distribution

along the THz-wave transmission path ( $r = 6 \text{ mm}$ ), the transmission path is shown by the red dotted line in Fig. 8(a). The electron density on the transmission path satisfies Gaussian distribution, which is similar to the distribution of the reentry plasma sheath [34], and the electron density at any point on the transport path increases with discharge voltage.

Fig. 9(a) shows the electron density distribution in the APPJ under a different needle electrode radius (discharge voltage is 5.0 kV). It can be seen from Fig. 8(a) that the electron density decreases with the increase of needle electrode radius, which is consistent with the related experimental results [35]. When the needle electrode radius increases from 0.25 to 0.75 mm, the electron density decreases from  $6.20 \times 10^{19} \text{ m}^{-3}$  to  $9.03 \times 10^{18} \text{ m}^{-3}$ . The effect of needle electrode radius on the electron density distribution on the THz-wave transmission path is analyzed in detail, as shown in Fig. 9(b). Although the electron density at any point on the transport path all decreases with the needle electrode radius, the change degree is much smaller than the electron density near the needle tip.

#### IV. PROPAGATION CHARACTERISTICS OF THz WAVE IN APPJ DEVICE

Based on the comparison and verification of the above electron density simulation and experimental results, the simulation results of propagation characteristics of the THz wave

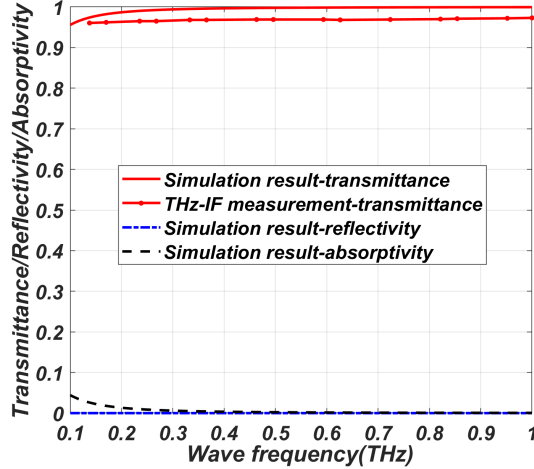


Fig. 10. Comparison of simulation results with THz-TDS experiment results at a discharge voltage of 4.0 kV.

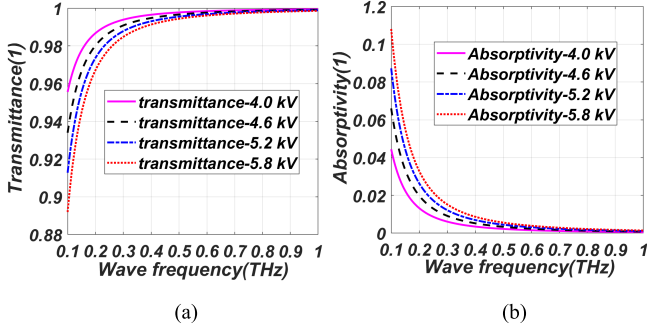


Fig. 11. Simulation results of THz-wave (a) transmittance and (b) absorptivity in APPJ under different discharge voltages.

in APPJ are compared with the experimental results of the THz-IF system, as shown in Fig. 10.

According to Fig. 10, the simulation results of the THz-wave transmittance in APPJ are in good agreement with the experimental results of the THz-IF system, both in terms of the transmittance variation trend with THz-wave frequency and the specific value. However, there are some differences between the two frequencies below 0.25 THz. The reason may be that the plasma jet is actually approximately cylindrical and the distribution is not uniform, and the scattering of the THz wave by the cylindrical nonuniform plasma in the actual THz-IF measurement leads to the small error between the simulated and measured curves.

In addition, the reflection coefficient of the THz wave in APPJ is almost 0, and the absorption coefficient changes inversely with the change of transmission coefficient, which indicates that the absorbing collision effects play a major role in the attenuation of THz waves in APPJ, and the reflection effect is almost negligible. As the wave frequency increases, the sum of THz-wave transmittance and absorptivity in APPJ is always equal to 1 (the reflection is almost 0), which verifies the energy conservation law satisfied in the interaction of the THz wave with the APPJ.

Fig. 11(a) shows that the transmittance of THz waves in APPJ decreases with the increase of discharge voltage under the same needle electrode radius, the reason is that higher

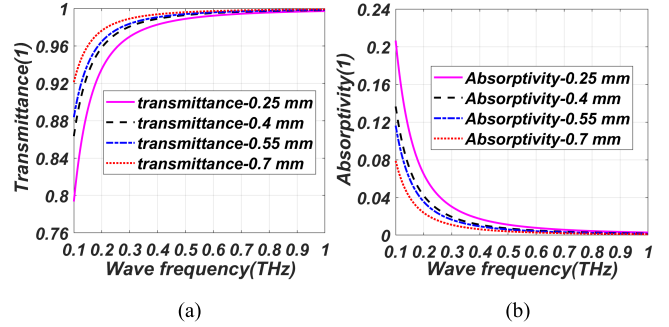


Fig. 12. Simulation results of THz-wave (a) transmittance and (b) absorption in APPJ under a different needle electrode radius.

discharge voltage leads to higher electron density and stronger absorption of THz wave. This phenomenon that a stronger absorption effect on THz waves with increasing voltages can be observed in Fig. 11(b). The THz-wave transmittance and absorption in the APPJ show an opposite trend for the increase of the needle electrode radius, as shown in Fig. 12. When the needle electrode radius was increased from 0.25 to 0.75 mm, THz-wave transmittance at 0.1 THz increased from 0.79 to 0.92, and the absorption increased from 0.21 to 0.08. With the increase of THz wave, the transmittance and absorptivity gradually are close to 1 and 0, respectively, which is due to the strong energy of high-frequency electromagnetic waves to penetrate the plasma.

Based on the analysis of the above results, the plasma distribution produced by APPJ meets the Gaussian distribution, the electron density is up to  $10^{19} \text{ m}^{-3}$ , and the plasma sheath thickness is about 5 mm, which is highly compatible with the plasma sheath environment around HIFIRE-5b vehicle. And through the theoretical and experimental research in APPJ, it is observed that the absorption effect plays a major role in the transmission characteristics of THz wave in APPJ, and the reflection effect can be almost ignored, which is consistent with the phenomenon observed in HIFIRE-5b vehicle in our previous research [14], [15]. The THz transmission research results in the APPJ verify the feasibility of the APPJ device used in the ground test for reentry communication research. More importantly, the theoretical model and THz-IF diagnostic method developed in this article are of great significance to the ground test verification of the reentry communication scheme for APPJ or plasma-jet-type wind tunnels in the future.

## V. CONCLUSION

A joint simulation model of APPJ discharge and THz propagation was developed to investigate the plasma characteristics and THz-wave propagation characteristics in atmospheric-pressure plasma jet, the electron density is verified by comparing THz-IF measurement results and reported experiment results by THz-TDS system, and the THz-wave transmission coefficient in APPJ is verified by comparison with the THz-IF experimental results. The simulation results show good agreement with the experimental results, which reveals the feasibility and accuracy of the joint simulation model.

Furthermore, the effects of different discharge voltages and needle electrode radius on the electron density and THz-wave

propagation characteristics in APPJ are discussed. The electron density increases with the discharge voltage, leading to a decrease in THz-wave transmittance. For the needle electrode radius, the electron density and THz-wave transmission are affected exactly opposite to the discharge voltage. Through further analysis of the reflection coefficient and absorption coefficient, it is concluded that the absorption effect plays a major role in the THz-wave transmission characteristics in APPJ, and the reflection effect can be almost ignored, which is consistent with the phenomenon observed in the HIFIRE-5b vehicle. In addition, electron density and plasma sheath thickness in APPJ can be adjusted by the discharge voltage or needle electrode radius, and pipe diameter, respectively. By changing these APPJ configurations, the plasma environment in the APPJ can be highly matched with the real reentry plasma sheath under different flight parameters and vehicle shapes, which will be further explored in the subsequent work.

#### ACKNOWLEDGMENT

The authors would like to thank the anonymous reviewers and editors for their valuable comments and suggestions to improve the quality of this article.

#### REFERENCES

- [1] B. Yao, X. Li, L. Shi, Y. Liu, and B. Bai, "A layered fluctuation model of electron density in plasma sheath and instability effect on electromagnetic wave at Ka band," *Aerosp. Sci. Technol.*, vol. 78, pp. 480–487, Jul. 2018.
- [2] Y. Y. Ding et al., "An analysis of radar detection on a plasma sheath covered reentry target," *IEEE Trans. Aerosp. Electron. Syst.*, vol. 57, no. 6, pp. 4255–4268, Dec. 2021.
- [3] B. A. Webb and R. W. Ziolkowski, "Metamaterial-inspired multilayered structures optimized to enable wireless communications through a plasmasonic region," *Appl. Phys. Lett.*, vol. 118, no. 9, Mar. 2021, Art. no. 094102.
- [4] W. Ouyang and Y. Liu, "Impact of ionization rate on the transmission of electromagnetic wave in realistic plasma," *Phys. Plasmas*, vol. 27, no. 3, Mar. 2020, Art. no. 033507.
- [5] A. V. Bogatskaya, N. V. Klenov, M. V. Tereshonok, S. S. Adjemov, and A. M. Popov, "Resonant interaction of electromagnetic wave with plasma layer and overcoming the radiocommunication blackout problem," *J. Phys. D, Appl. Phys.*, vol. 51, no. 18, 2018, Art. no. 185602.
- [6] S. Sun, S. Liu, and S. Zhong, "Analysis of terahertz wave penetration capacity to 2D conductive cylinder coated with steady-state parabolic distribution plasma media," *Results Phys.*, vol. 27, Aug. 2021, Art. no. 104516.
- [7] K. Sengupta, T. Nagatsuma, and D. M. Mittleman, "Terahertz integrated electronic and hybrid electronic-photonic systems," *Nature Electron.*, vol. 65, no. 2, pp. 622–635, 2019.
- [8] M. Zhu, J. Zhang, J. Yu, and X. You, "Demonstration of record-high 352-Gbps terahertz wired transmission over hollow-core fiber at 325 GHz," *Sci. China Inf. Sci.*, vol. 65, no. 2, Feb. 2022, Art. no. 127301.
- [9] Y. Tian, Y. Han, Y. Ling, and X. Ai, "Propagation of terahertz electromagnetic wave in plasma with inhomogeneous collision frequency," *Phys. Plasmas*, vol. 21, Feb. 2014, Art. no. 023301.
- [10] J. Chen, K. Yuan, L. Shen, X. Deng, L. Hong, and M. Yao, "Studies of terahertz wave propagation in realistic reentry plasma sheath," *Prog. Electromagn. Res.*, vol. 157, pp. 21–29, 2016.
- [11] K. Yuan et al., "Sub-THz signals' propagation model in hypersonic plasma sheath under different atmospheric conditions," *Sci. China Inf. Sci.*, vol. 60, no. 11, 2017, Art. no. 113301.
- [12] X. Yang, B. Wei, and W. Yin, "Relationship between the velocity of hypersonic vehicles and the transmission efficiency of radio waves," *Waves Random Complex Media*, vol. 29, no. 2, pp. 382–391, Apr. 2019.
- [13] Q. F. Zhang, Y. P. Han, Q. L. Dong, and C. Dong, "Analysis of the influence of sheath positions, flight parameters and incident wave parameters on the wave propagation in plasma sheath," *Plasma Sci. Technol.*, vol. 24, no. 3, 2022, Art. no. 035003.
- [14] R. X. Tang, Z. F. Xiong, K. Yuan, M. Y. Mao, Y. H. Wang, and X.H. Deng, "EHF wave propagation in the plasma sheath enveloping sharp-coned hypersonic vehicle," *IEEE Antennas Wireless Propag. Lett.*, vol. 20, no. 6, pp. 978–982, Jun. 2021.
- [15] W. C. Ouyang, Q. Liu, and Z. W. Wu, "Difference analysis in the terahertz wave propagation in thermochemical nonequilibrium plasma sheath under different hypersonic vehicle shapes," *Chin. J. Aeronaut.*, pp. 1–15, Nov. 2022.
- [16] D. Jang, H. S. Uhm, D. Jang, M. S. Hur, and H. Suk, "Electron density characterization of inductively-coupled argon plasmas by the terahertz time-domain spectroscopy," *Plasma Sources Sci. Technol.*, vol. 25, no. 6, Oct. 2016, Art. no. 065008.
- [17] N. P. Brown, S. J. Grauer, J. A. Deibel, M. L.R. Walker, and A. M. Steinberg, "Bayesian framework for THz-TDS plasma diagnostics," *Opt. Exp.*, vol. 29, no. 4, pp. 4887–4901, 2021.
- [18] J. H. Sun et al., "Propagation characteristics of terahertz wave in inductively coupled plasma," *Opt. Exp.*, vol. 29, no. 22, pp. 35837–35847, 2021.
- [19] W. Ouyang, C. Ding, Q. Liu, W. Deng, and Z. Wu, "Effect of material properties on electron density and electron energy in helium atmospheric pressure plasma jet," *Results Phys.*, vol. 33, Feb. 2022, Art. no. 105215.
- [20] Y. Liu, Z. Tan, X. Wang, X. Li, and X. Chen, "Investigation on the effects of the operating conditions on electron energy in the atmospheric-pressure helium plasma jet," *Phys. Plasmas*, vol. 26, no. 4, Apr. 2019, Art. no. 043506.
- [21] K. Chen, D. Xu, J. Li, X. Geng, K. Zhong, and J. Yao, "Application of terahertz time-domain spectroscopy in atmospheric pressure plasma jet diagnosis," *Results Phys.*, vol. 16, Mar. 2020, Art. no. 102928.
- [22] W. D. Liu et al., "An overview of diagnostic upgrade and experimental progress in the KTX," *Nucl. Fusion*, vol. 59, no. 11, 2019, Art. no. 112013.
- [23] G. J. M. Hagelaar and L.C. Pitchford, "Solving the Boltzmann equation to obtain electron transport coefficients and rate coefficients for fluid models," *Plasma Sources Sci. Technol.*, vol. 14, no. 4, p. 722, 2005.
- [24] J. A. Bittencourt, *Fundamentals of Plasma Physics*, 3rd ed. New York, NY, USA: Springer-Verlag, 2004.
- [25] Y. Morabit, R. D. Whalley, E. Robert, M. I. Hasan, and J. L. Walsh, "Turbulence and entrainment in an atmospheric pressure dielectric barrier plasma jet," *Plasma Processes Polym.*, vol. 17, no. 6, Jun. 2020, Art. no. 1900217.
- [26] A. V. Omran et al., "Cold atmospheric single plasma jet for RONS delivery on large biological surfaces," *Plasma Sources Sci. Technol.*, vol. 29, no. 10, 2020, Art. no. 105002.
- [27] A. Bourdon et al., "Numerical and experimental study of the dynamics of a  $\mu$ s helium plasma gun discharge with various amounts of  $N_2$  admixture," *Plasma Sources Sci. Technol.*, vol. 25, no. 3, 2016, Art. no. 035002.
- [28] T. Darny, J.-M. Pouvesle, V. Puech, C. Douat, S. Dozias, and E. Robert, "Analysis of conductive target influence in plasma jet experiments through helium metastable and electric field measurements," *Plasma Sources Sci. Technol.*, vol. 26, no. 4, Mar. 2017, Art. no. 045008.
- [29] J. L. Xie et al., "Design of interferometer system for Keda Torus eXperiment using terahertz solid-state diode sources," *Rev. Sci. Instrum.*, vol. 85, Jul. 2014, Art. no. 11D828.
- [30] W. Z. Mao et al., "Measurement of density profile and fluctuations using a multi-channel terahertz solid-state interferometer system on Keda Torus eXperiment (KTX)," *Rev. Sci. Instrum.*, vol. 92, no. 5, 2021, Art. no. 053514.
- [31] X.N. Geng, "Study on the propagation characteristics of terahertz wave in plasma," M.S. dissertation, Tianjin Univ., Tianjin, China, 2019, doi: [10.27356/d.cnki.gjtu.2019.003675](https://doi.org/10.27356/d.cnki.gjtu.2019.003675).
- [32] Z. Niu et al., "Characteristics of nanosecond-pulse atmospheric pressure plasma jet," *High Power Laser Part. Beams*, vol. 24, no. 3, pp. 617–620, 2012.
- [33] G. V. Naidis, "Modeling of helium plasma jets emerged into ambient air: Influence of applied voltage, jet radius, and helium flow velocity on plasma jet characteristics," *J. Appl. Phys.*, vol. 112, no. 10, Nov. 2012, Art. no. 103304.
- [34] W. Ouyang, T. Jin, Z. Wu, and W. Deng, "Study of terahertz wave propagation in realistic plasma sheath for the whole reentry process," *IEEE Trans. Plasma Sci.*, vol. 49, no. 1, pp. 460–465, Jan. 2021.
- [35] B. W. Feng, R. Y. Wang, Y. P. X. Ma, and X.X. Zhong, "Evolution of electron density of pin-to-plate discharge plasma under atmospheric pressure," *Acta Phys. Sinica*, vol. 70, no. 9, 2021, Art. no. 095201.



**Wenchong Ouyang** (Graduate Student Member, IEEE) received the B.E. degree from the Guilin University of Electronic Technology, Guilin, China, in 2017, and the M.S. degree from Xidian University, Xi'an, China, in 2020. He is currently pursuing the Ph.D. degree with the University of Science and Technology of China, Hefei, China.

His research interests are focused on the terahertz communication, blackout problem, and plasma medicine.



**Shuzhan Gao** received the B.S. degree from Qingdao University, Qingdao, China, in 2018. He is currently pursuing the M.S. degree with the University of Science and Technology of China, Hefei, China.

His current research interests include plasma source diagnostic, plasma application, and interaction of electromagnetic waves and plasma.



**Qi Liu** received the B.S. degree from Lanzhou University, Lanzhou, China, in 2019. He is currently pursuing the Ph.D. degree with the University of Science and Technology of China, Hefei, China.

His current research interests include plasma source diagnostic, plasma application, and plasma gas-liquid interaction.



**Wenzhe Mao** received the B.S. and Ph.D. degrees from the University of Science and Technology of China, Hefei, China, in 2008 and 2014, respectively.

From June 2014 to August 2016, he was a Post-Doctoral Researcher at the University of Science and Technology of China. Since September 2018, he has been a Special Associate Researcher at the University of Science and Technology of China. His current research interests include magnetic fluid instabilities and diagnostics of high-temperature plasmas in fusion devices.



**Zhengwei Wu** (Member, IEEE) received the B.S. and M.S. degrees from the University of Science and Technology of China, Hefei, China, in 2000 and 2005, respectively, and the Ph.D. degree from the City University of Hong Kong, Kowloon, Hong Kong, and in collaboration with The University of Sydney, Sydney, NSW, Australia, in 2010.

From February 2010 to August 2014, he was a Researcher at the City University of Hong Kong. From September 2014 to September 2017, he was the Director of the Scientific Research Department at the Hefei Institute of Public Security, Tsinghua University, Beijing, China. Since October 2017, he has been with the University of Science and Technology of China, where he is currently a specially appointed Researcher.